Journal of Materials Chemistry B

PAPER

View Article Online
View Journal | View Issue

Cite this: J. Mater. Chem. B, 2019, 7, 7540

Redox-responsive tetraphenylethylene-buried crosslinked vesicles for enhanced drug loading and efficient drug delivery monitoring†

Yunlong Yu,[a] Yun Chen,[a] Jingsheng Huang,[a] Liang Wang,[a] Zhongwei Gu[b] and Shiyong Zhang *[a]

Received 3rd August 2019,
Accepted 25th October 2019

DOI: 10.1039/c9tb01639b

rsc.li/materials-b

Liposomes have been applied extensively as nanocarriers in the clinic (*e.g.*, to deliver anticancer drugs) due to their biocompatibility and internal cavity structures. However, their low drug-loading capacity (DLC; <10%) and uncontrolled release reduce their efficacy in cancer treatment. To improve the DLC and monitor release of drugs in cells in real-time, stimuli-responsive vesicles must be developed. We present various amphiphilic tetraphenylethylene (TPE)-containing compounds designed to self-assemble into liposome-like vesicles that can load both hydrophilic and hydrophobic drugs. The highest DLC for doxorubicin (DOX) was ≤26% for vesicles (diameter = 105 nm) that could encapsulate hydrophilic DOX in the interior water pool and hydrophobic DOX *via* π–π stacking interactions between DOX and the TPE moiety. The stable vesicles could respond rapidly to overexpressed glutathione in the tumor microenvironment to release loaded DOX for cancer therapy. Vesicles modified by active targeting groups showed more efficacious tumor treatment compared with unmodified vesicles and free DOX *in vitro* and *in vivo*. Simultaneously we observed, spatiotemporally, the subcellular location of the delivery system and release process of DOX. Our work provides a novel nano-engineering technology to integrate the desired properties for anticancer theranostics: high DLC, stability, stimuli-responsiveness to the cancer environment, drug-delivery monitoring, active targeting, and suppression of tumor growth. These novel vesicles could be employed as multifunctional drug-delivery systems for cancer therapy.

1. Introduction

Driven by developments in nanotechnology in recent decades, there have been great breakthroughs in biomedical treatment for the simultaneous diagnosis and therapy of cancers or other diseases.[1–3] Notably, nano-based drug-delivery vesicles have been applied to deliver various components due to the existence of specific structures.[2,4,5] Thus, they play crucial parts in theranostic applications. Liposome vesicles with lipid bilayer-like structures have been approved as doxorubicin (DOX) carriers in anticancer treatment to reduce the toxicity of the free drug *in vivo*, and include Doxil/Caelyx, DaunoXome, Myocet and EVACET.[6,7] However, as reported, the low drug-loading capacity (<10%) restricts the drug content and true therapeutic effect considerably.[8,9] Moreover, with liposomes, just as vehicles carrying hydrophilic drugs, one cannot monitor in real-time drug release during delivery.[10] In addition, the uncontrolled release of liposomes may also cause toxicity to normal cells and even induce drug resistance.[11] Therefore, designing stimuli-responsive liposome-like nanocarrier systems for enhancing therapeutic drug loading, controlled release, and monitoring drug localization and the process of release is important.

Fluorescent dyes have been applied extensively for optoelectronics, cell imaging, diagnostic sensors, and targeted drug delivery.[12–14] However, luminescence can be quenched by the integration or encapsulation of fluorescent dyes in nanostructures because of the notorious aggregation-caused quenching (ACQ) effect.[15] To overcome these drawbacks, aggregation-induced emission (AIE) molecules have been employed for biosensing and bioimaging due to their special ability to aggregate and luminesce.[12,16,17] If they are well dispersed, only weak luminescence can be obtained. Once aggregation occurs or a solid state is formed, high emission occurs. As reported previously, AIE materials show great potential application in cell imaging and disease detection.[17,18] For example, Liang *et al.*[18] directly mixed AIE molecules with DOX to form nanoparticles (NPs) for drug-delivery monitoring and cancer treatment. However, the NP morphology was determined by the DOX molar ratio

[a] National Engineering Research Center for Biomaterials, College of Chemistry, Sichuan University, 29 Wangjiang Road, Chengdu 610064, China. E-mail: szhang@scu.edu.cn; Fax: +86-28-85411109; Tel: +86-28-85411109
[b] College of Materials Science and Engineering, Nanjing Tech University, Nanjing, Jiangsu 210009, China

† Electronic supplementary information (ESI) available. See DOI: 10.1039/c9tb01639b

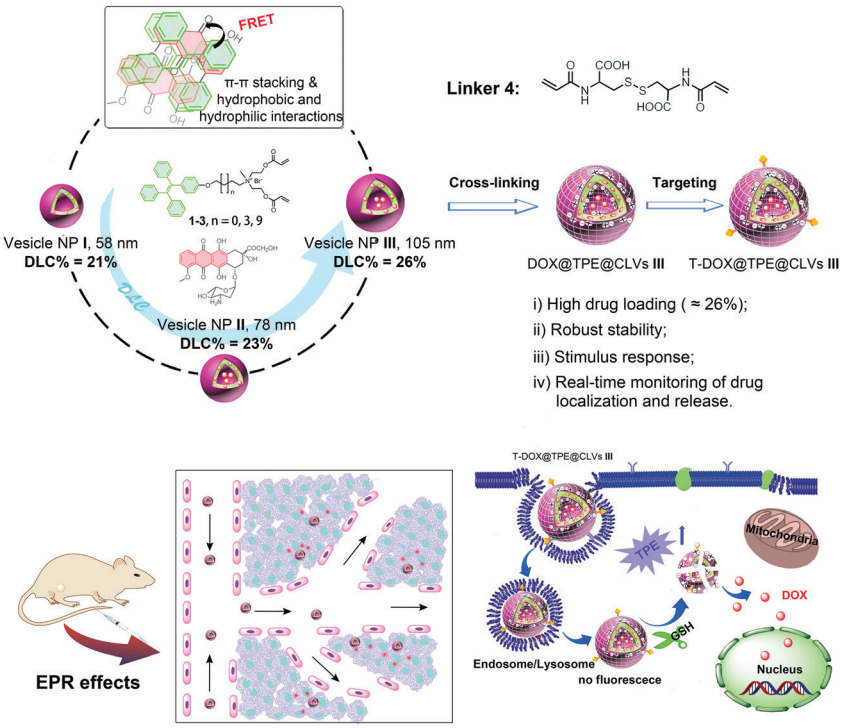

Scheme 1 Preparation of DOX@TPE@CLVs **I–III** and T-DOX@TPE@CLVs **III** for efficacious anticancer therapy (schematic).

so that only a small DOX loading content (10%) would be achieved. Our research team has long-term experience of the design and synthesis of crosslinked small-molecule vesicles, which contain hydrophilic water pools and hydrophobic bilayers and have great potential to improve the drug-loading capacity.[19–21] Also, these vesicles can be designed with functional groups for control of sizes, zeta potential, cell targets and stimulus response to tumor microenvironments. Therefore, our small-molecule vesicles hold great potential to work as drug-delivery systems for cancer therapy.

We report the synthesis of a series of amphiphilic tetraphenylethylene (TPE)-buried compounds **1–3** which can self-assemble into different-sized vesicles TPE@LVs **I**, **II** and **III** (58, 78 and 105 nm, respectively) (Scheme 1). The new drug-delivery system could encapsulate hydrophilic and hydrophobic DOX by hydrophilic cavities and hydrophobic bilayers *via* π–π stacking. The highest drug-loading content (DLC) could be ≤26% using TPE@LVs **III**. After crosslinking, the resulting DOX@TPE@CLVs **III** displayed good stability in various environments and during long circulation times in blood. Being responsive to the tumor microenvironment, the vesicles could be broken to release the encapsulated DOX. After modification with active targeting glucose, T-DOX@TPE@CLVs **III** showed good targeting and chemotherapy to suppress the growth of HepG2 cancer cells *in vitro* and *in vivo*. As an ideal nanoplatform, utilization of the vesicles also enabled real-time monitoring of drug localization during the entire process of drug delivery. Therefore, a smart redox-responsive drug-delivery system was fabricated for fluorescent vesicles which could provide new opportunities for delivery of chemotherapeutic agents for multifunctional applications in the clinic.

2. Results and discussion

The synthetic details of tetraphenylethylene-buried amphiphiles **1–3** are described in ESI.† After self-assembly in water, vesicles were formed directly. As shown in Fig. 1, the hydrodynamic sizes of TPE@LVs **I–III** vesicles varied from 58 nm to 105 nm with extension of the alkyl length, which was detected by dynamic light scattering (DLS). Notably, the sizes from transmission electron microscopy (TEM) were smaller than obtained by DLS because the vesicles shrank after being dried for TEM. The vesicle structures of TPE@LVs **I–III** were confirmed by an assay measuring carboxyfluorescein (CF) leakage (Fig. S2, ESI†). Due to their lipid bilayer-like structure, the vesicles could encapsulate hydrophilic drugs in the hydrophilic water pool and hydrophobic drugs in the hydrophobic shell layer. Here, we used hydrophilic DOX and deacidified DOX (hydrophobic) as drug models. TPE@LVs **I–III** vesicles could deliver both types of DOX simultaneously. As shown in Fig. 1e, the DLC increased from 21% to 26% along with different sizes *via* π–π stacking interactions between DOX and the TPE moiety;[18] the DLC was much higher than that of general liposomes (<10%). The encapsulation efficiency (EE) increased from 77% to 87% for the three vesicles. As reported, NP sizes of ~100 nm have the lowest plasma clearance rate and long circulation lifetimes.[8] For subsequent experiments, we selected TPE@LVs **III** vesicle as an optimal nanocarrier due to the highest DLC achieved and potential longest circulation time.

Crosslinking is a reliable strategy to stabilize nanocarriers for drug delivery. Here, linker **4** was used as a crosslinker to covalently bond the vesicles (TPE@CLVs **III**) to enhance the stability.

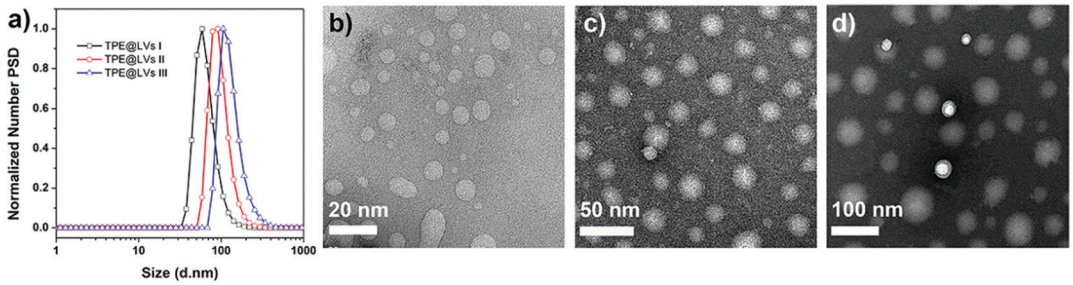

e)

Drug-carrier	DLC (loading hydrophilic DOX)	DLC (loading hydrophobic DOX)	DLC (Total)	EE (Total)
TPE@LVs **I**	11%	10%	21%	77%
TPE@LVs **II**	12%	11%	23%	81%
TPE@LVs **III**	14%	12%	26%	87%

Fig. 1 Characterization of the self-assembly of TPE-buried amphiphile **1–3** in water. (a) Distribution of the hydrodynamic diameters of compound **1–3**-fabricated TPE@LVs **I–III** in water, respectively. (b–d) TEM images of TPE@LVs **I–III** in sequence. (e) The drug-loading content (DLC) and encapsulation efficiency (EE) of nanoparticles TPE@LVs **I–III** to load DOX are summarized in the table.

After crosslinking, the size and spherical morphology of the vesicles did not change much, as observed from DLS and TEM in Fig. 2a. Proton nuclear magnetic resonance (^{1}H NMR) spectroscopy before and after crosslinking (Fig. S3, ESI†) showed that the characteristic peak of acrylate at 6.0–6.8 ppm disappeared, indicating successful conjugation with linker **4** (0.5 equiv.). The zeta potential measured on the vesicles changed from positive to approximately neutral after crosslinking, which provided further evidence of the formation of TPE@CLVs **III**. The low zeta potential worked aided long circulation times because it reduced the clearance by macrophages in blood during drug delivery. The dilution and FBS stability of TPE@CLVs **III** was evaluated using uncrosslinked (TPE@LVs)

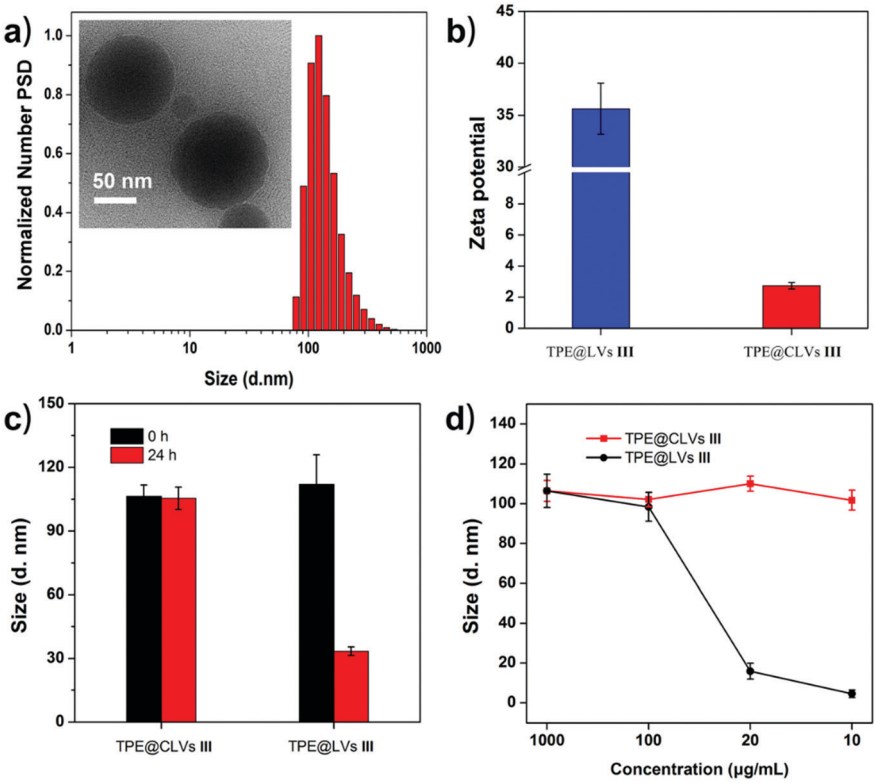

Fig. 2 Physicochemical properties of crosslinked TPE@CLVs **III**. (a) DLS and TEM of TPE@CLVs **III**. (b) Zeta potentials of uncrosslinked TPE@LVs **III** and crosslinked TPE@CLVs **III**. (c) Particle sizes of TPE@LVs **III** and TPE@CLVs **III** after incubation with 10% FBS at 37 °C over time ([**3**] = 200 μg mL^{-1}). (d) Particle sizes of TPE@LVs **III** and TPE@CLVs **III** at various dilutions at 37 °C.

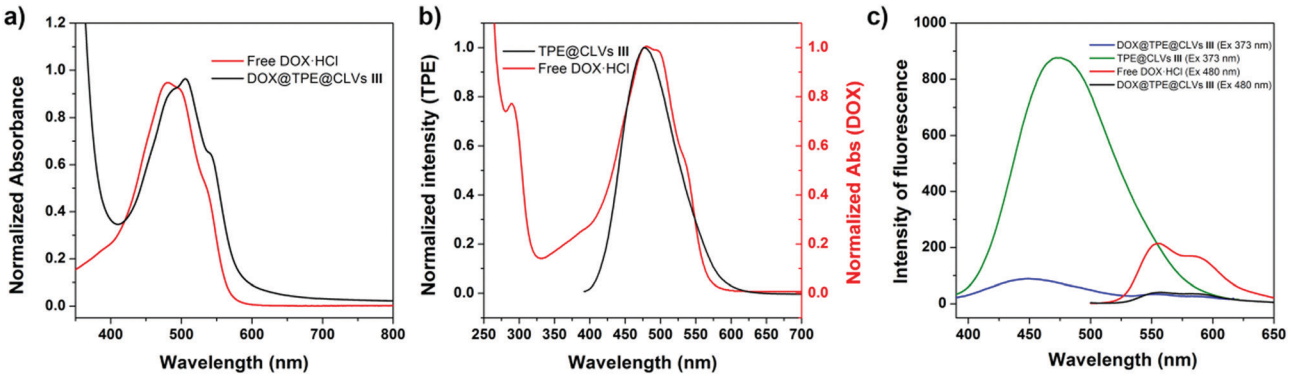

Fig. 3 (a) UV-vis absorption spectra of free DOX and DOX@TPE@CLVs **III**. (b) Fluorescence spectra of DOX@TPE@CLVs **III** and UV-vis absorption spectra of free DOX. (c) Fluorescence spectra of free DOX, TPE@CLVs **III** and DOX@TPE@CLVs **III** (TPE λ_{ex} = 373 nm, DOX λ_{ex} = 480 nm, [TPE] = 50 μM, [DOX] = 10 μg mL^{-1}).

as a comparison (Fig. 2c and d). The dimension of TPE@CLVs was unchanged even at a concentration below the critical vesicle concentration (CVC) whereas TPE@LVs disassembled during dilution. TPE@CLVs also showed good stability in 10% FBS for ≥24 h.

To characterize the interior composition of TPE@LVs **III** vesicles, fluorescence spectroscopy and UV-vis absorption spectroscopy were undertaken to explore the π–π interactions between DOX and TPE.[11,18] An absorption peak at 480 nm for free DOX in water was noted (Fig. 3a). After encapsulation in crosslinked vesicles, the formed DOX@TPE@CLVs **III** showed a red shift of the absorption peak to 506 nm, which was attributed to the ground-state electron donor–electron acceptor interaction and π–π stacking between TPE and DOX.[18] The overlap of the emission spectrum of TPE and the absorption spectrum of DOX (Fig. 3b) indicated a Förster resonance energy transfer (FRET) effect. After loading DOX in TPE@CLVs **III**, the emission of DOX@TPE@CLVs **III** decreased markedly at 475 nm and 556 nm compared with that of TPE@LVs **III** and free DOX respectively due to the FRET effect and self-quenching of DOX aggregation.[18] However, once DOX had been released from the vesicles, TPE fluorescence recovered gradually with time (Fig. S4, ESI†). Therefore, DOX@TPE@CLVs **III** could be applied to realize real-time monitoring of the localization and release of drugs upon internalization into cancer cells.

Next, the stimuli-responsive release of DOX@TPE@CLVs **III** was evaluated under various environments (Fig. 4). At pH = 7.4, there was only 19% release of DOX, and a slight increase in DOX release at pH = 5.0, which might have occurred because the acidic environment changed part of the hydrophobic DOX to acidified DOX (hydrophilic). Only in the presence of glutathione (GSH) could >60% of DOX be released in 35 h, whereas 80% release could be achieved under acidic conditions. The DOX@TPE@CLVs **III** system was designed to respond to the overexpressed GSH (2–10 mM) in the tumor microenvironment.[22,23] Thus, redox-labile DOX@TPE@CLVs **III** could be broken down by removal of disulfide bonds by GSH to release the loaded DOX. Vesicle damage could be detected through size variation by DLS (Fig. 4b). These results implied that DOX@TPE@CLVs **III** were practical and favorable for stimuli-responsive release of anticancer drugs *in vitro*.

For efficacious anticancer treatment, specific targeting of tumor cells is important.[20,24,25] Here, DOX@TPE@CLVs **III** was modified with 20 mol% glucose by a one-step reaction with

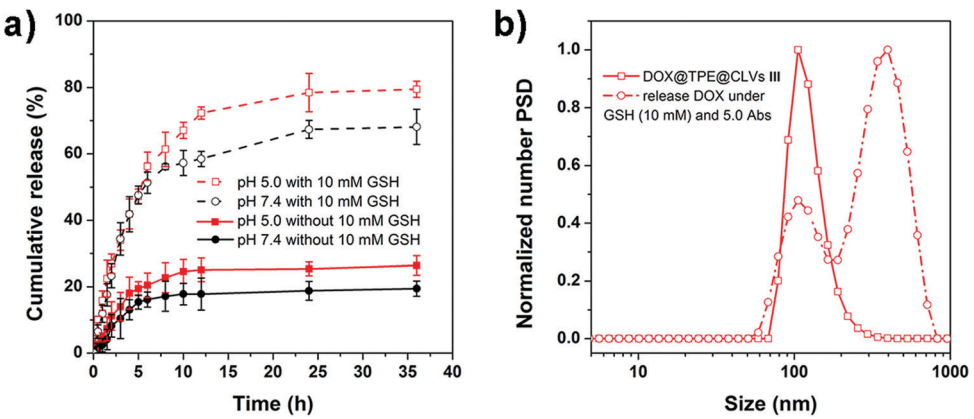

Fig. 4 (a) *In vitro* DOX release of crosslinked DOX@TPE@CLVs **III** at pH = 7.4 (PBS buffer) and pH = 5.0 (acetate buffer) at 37 °C over time. (b) Variation in particle size of TPE@CLVs **III** before and after incubation at pH = 5.0 (acetate buffer) and 10 mM glutathione (GSH) at 37 °C.

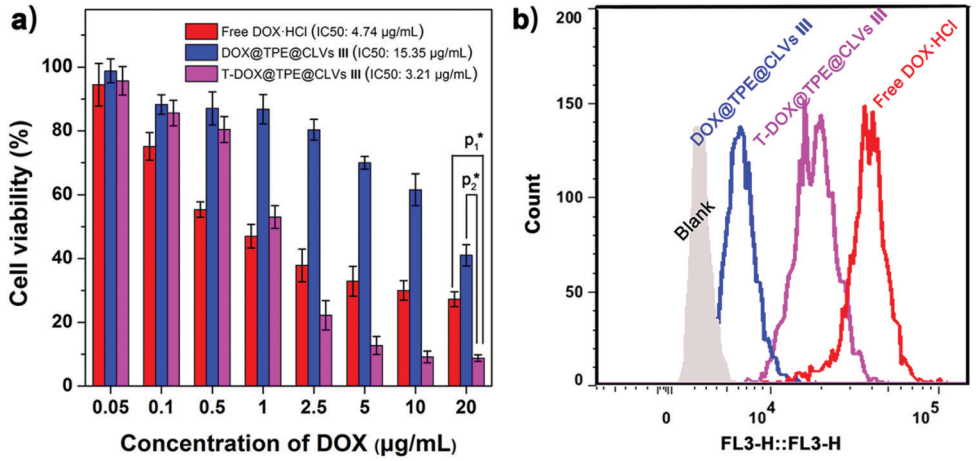

Fig. 5 (a) Viability of HepG2 liver cells after incubation with free DOX·HCl, DOX@TPE@CLVs **III** or T-DOX@TPE@CLVs **III** for 24 h at 37 °C at a series of concentrations (mean ± SD, n = 5, P_1* < 0.05, P_2* < 0.05). (b) Quantification of cellular uptake of free DOX·HCl, DOX@TPE@CLVs **III** and T-DOX@TPE@CLVs **III** after incubation for 3 h ([DOX] = 2 μM) by flow cytometry.

carboxylic-acid groups on vesicles to form T-DOX@TPE@CLVs **III**. To evaluate cytotoxicity *in vitro*, free DOX·HCl, DOX@TPE@CLVs **III** and T-DOX@TPE@CLVs **III** were incubated separately with HepG2 liver cancer cells and the Cell Counting Kit (CCK)-8 assay carried out (Fig. 5a). After 24 h of treatment, the half-maximal inhibitory concentration (IC_{50}) of DOX@TPE@CLVs **III** was 15.35 μg mL^{-1}, which was higher than that of free DOX·HCl (4.74 μg mL^{-1}). The zeta potential for TPE@CLVs **III** was low (Fig. 2), which could affect the endocytosis of cells. Free DOX could diffuse rapidly into cancer cells to kill them. Encouragingly, for T-DOX@TPE@CLVs **III**, a low IC_{50} could be obtained, 3.21 μg mL^{-1}, which was even lower than that for free DOX. T-DOX@TPE@CLVs **III** could target and enter cells effectively. After the response to GSH and in acidic environment, the vesicles ruptured to release DOX to cause cytotoxicity. Subsequently, flow cytometry was applied to estimate the intracellular DOX concentration after cell uptake. As shown in Fig. 5b, the T-DOX@TPE@CLVs **III** was more efficient in delivering DOX molecules into cells compared with DOX@TPE@CLVs **III**, data that were consistent with the results of cytotoxicity testing.

To observe the subcellular locations of the drug-delivery system directly, TPE@CLVs **III**, free DOX·HCl, DOX@TPE@CLVs **III** and T-DOX@TPE@CLVs **III** were incubated with HepG2 cells for 3, 6 and 12 h, respectively, and observed by confocal laser scanning microscopy. Blue fluorescence (480 nm) was attributed to the TPE moiety and red fluorescence (576 nm) to DOX molecules (Fig. 6). Free DOX·HCl could enter cells through diffusion, and strong fluorescence was observed in nuclei after incubation with HepG2 cells for 6 h. TPE@CLVs **III** was present only in the cytoplasm even after 12 h incubation. For DOX@TPE@CLVs **III** and T-DOX@TPE@CLVs **III**, weak fluorescence appeared after 3 h incubation with HepG2 cells due to ACQ and the FRET effect. After incubation time for 6 and 12 h, the fluorescence from TPE and DOX recovered gradually as a result of the disassembly of NP structure to release DOX. T-DOX@TPE@CLVs **III** could enter cells faster than DOX@TPE@CLVs **III** for specific active targeting. In particular, 12 h after incubation, T-DOX@TPE@CLVs **III** showed stronger fluorescence because more DOX was released and entered the cytoplasm and nuclei. These results suggested that this nanocarrier could be

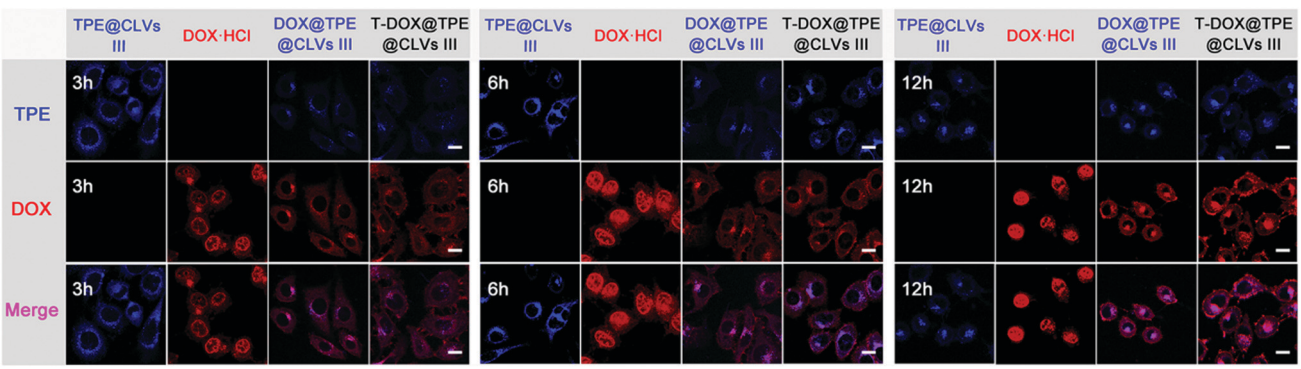

Fig. 6 CLSM images of HepG2 cells treated with free DOX·HCl, TPE@CLVs **III**, DOX@TPE@CLVs **III** or T-DOX@TPE@CLVs **III** for 3, 6, or 12 h. For each panel, the fluorescence of TPE in cells (blue), fluorescence of DOX in cells (red) and merged fluorescence (pink) are shown. Scale bar = 10 μm ([DOX] = 4 μM, [**1**] = 11.6 μM).

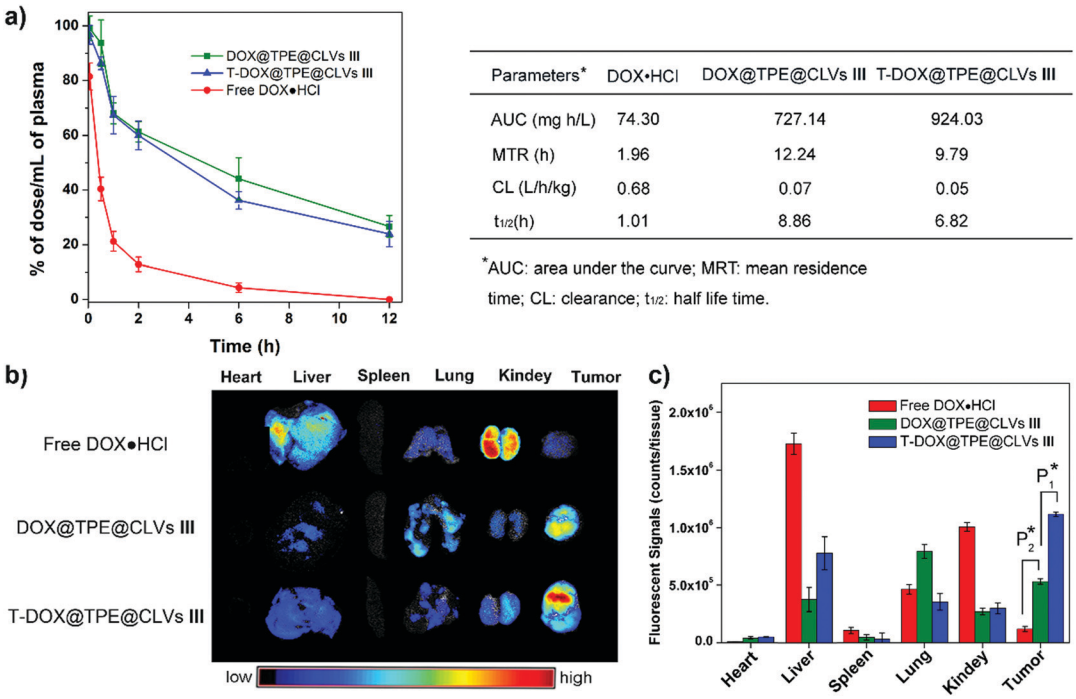

Parameters*	DOX•HCl	DOX@TPE@CLVs III	T-DOX@TPE@CLVs III
AUC (mg h/L)	74.30	727.14	924.03
MTR (h)	1.96	12.24	9.79
CL (L/h/kg)	0.68	0.07	0.05
$t_{1/2}$(h)	1.01	8.86	6.82

*AUC: area under the curve; MRT: mean residence time; CL: clearance; $t_{1/2}$: half life time.

Fig. 7 *Ex vivo* fluorescence images showing the pharmacokinetics of DOX·HCl, DOX@TPE@CLVs **III** and T-DOX@TPE@CLVs **III**. (a) Pharmacokinetic profiles after intravenous injection of samples in BALB/c mice (5 mg per kg bodyweight). (b) *Ex vivo* fluorescence images of tissues of HepG2 tumor-bearing nude mice 12 h after intravenous injection of DOX·HCl, DOX@TPE@CLVs **III** or T-DOX@TPE@CLVs **III**, respectively. (c) Quantitative analyses of the fluorescence intensity of tissues 12 h after injection, respectively (mean ± SD, n = 3).

applied to monitor the entire process of drug release for a drug-delivery system.

Furthermore, pharmacokinetic investigation *in vivo* was conducted using BALB/c mice bearing HepG2 solid tumors. After intravenous injection of DOX·HCl, DOX@TPE@CLVs **III** or T-DOX@TPE@CLVs **III**, plasma was collected for analyses. As illustrated in Fig. 7a, blood clearance of DOX@TPE@CLVs **III** and T-DOX@TPE@CLVs **III** was slower than that for free DOX·HCl. For free DOX, the area under the curve (AUC) was 74.30 and half-life ($t_{1/2}$) was 1.01 h, and DOX@TPE@CLVs **III** increased the AUC to 727.14 (9.78-fold) and increased $t_{1/2}$ to 8.86 h (8.77-fold). Moreover, the AUC and $t_{1/2}$ of T-DOX@TPE@CLVs **III** was 924.03 (12.44-fold) and 6.82 h (36.75-fold) compared with free DOX·HCl. A drug-biodistribution study was carried out *in vivo* to estimate the antitumor activity of free DOX·HCl, DOX@TPE@CLVs **III** and T-DOX@TPE@CLVs **III**. As shown in Fig. 7b, analyses of fluorescence intensity indicated that the crosslinked NPs targeted the tumors in living mice passively *via* the enhanced permeability and retention (EPR) effect. According to *ex vivo* images and semiquantitative analyses of DOX content in different organs and tumors (λ_{ex} = 480 nm, λ_{em} = 580 nm), free DOX·HCl accumulated readily in the liver and kidneys, whereas T-DOX@TPE@CLVs **III** was the predominant delivery system for active targeting of solid tumors even 12 h after injection (Fig. 7c).

To evaluate the therapeutic efficacy of free DOX·HCl, DOX@TPE@CLVs **III** and T-DOX@TPE@CLVs **III** *in vivo*, nude mice bearing HepG2 solid tumors were applied. The volume of tumor in living mice was measured continuously for 18 days. As shown in Fig. 8a, the volume of the tumor region on T-DOX@TPE@CLVs **III**-treated mice showed much slower growth than that for saline (~9.9 ± 0.3 fold)-, free DOX·HCl (~7.2 ± 0.4 fold)- and DOX@TPE@CLVs **III** (~1.5 ± 0.4 fold)-treated mice. Upon killing after 18 days, the typical images and weights of tumors are shown as Fig. 8b and c, respectively. Meanwhile, the relative change in bodyweight was also measured (Fig. 8d). Clearly, the bodyweight of mice treated with free DOX·HCl decreased to ~66% due to its side effects.[8,26] Others groups showed relatively stable bodyweights of mice. Based on tests in mice, T-DOX@TPE@CLVs **III** could suppress tumor growth *in vivo*, which agreed with the corresponding results *in vitro*.

3. Conclusions

We designed and synthesized amphiphilic TPE-bearing compounds to self-assemble liposome-like vesicles: TPE@LVs. They could be applied to deliver both hydrophilic DOX in the water pool and hydrophobic DOX in the bilayer *via* π–π stacking interactions between DOX and the TPE moiety. The highest DLC of 26% was achieved using a vesicle diameter of 105 nm, which was higher than that of general liposomes (<10%). After crosslinking, the formed DOX@TPE@CLVs not only showed robust stability under physiological conditions, but also responded to the tumor microenvironment to release DOX for cancer therapy. After modification with active targeting glucose molecules, T-DOX@TPE@CLVs could be effectively applied to monitor

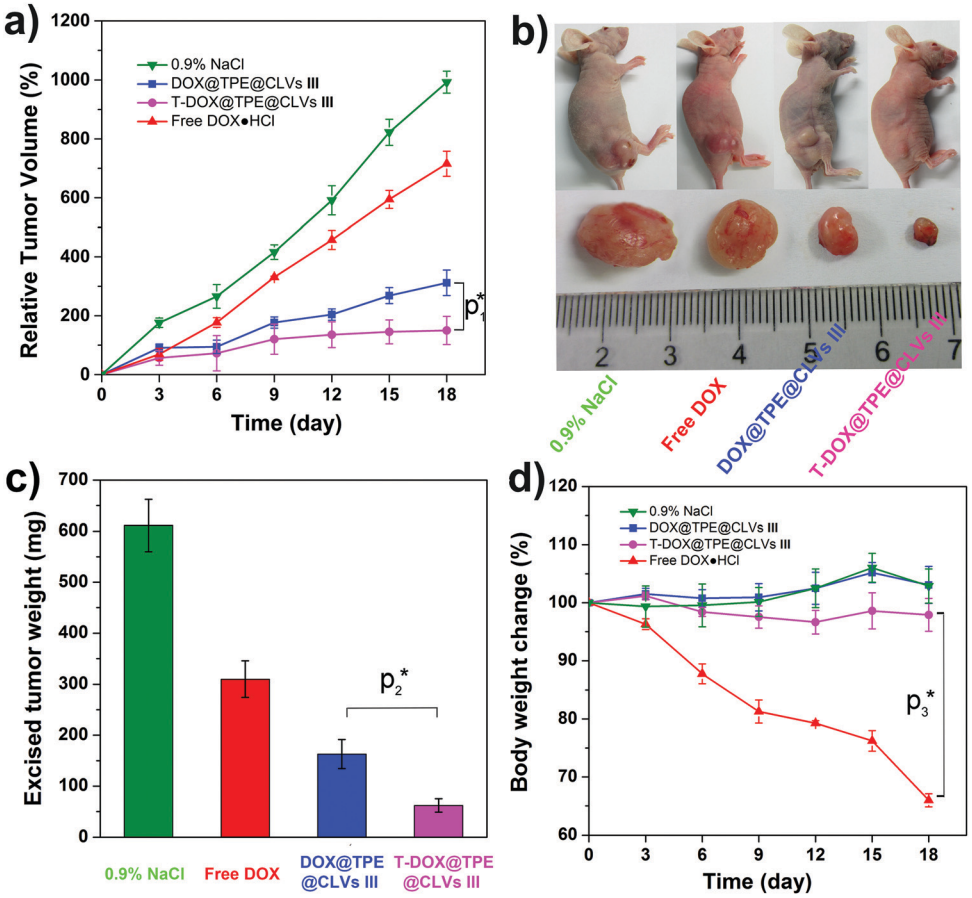

Fig. 8 *In vivo* anticancer therapy using free DOX·HCl, DOX@TPE@CLVs **III** and T-DOX@TPE@CLVs **III** and the control (0.9% NaCl) after intravenous injection through the tail vein of nude mice bearing xenograft HepG2 liver tumors. (a) Relative change in the tumor volume over time (mean ± SD, n = 5, P_1* < 0.05). (b) Representative image of mice bearing tumors and excised tumors after treatment for 18 days. (c) The excised tumor weights after treatment with 0.9% saline, free DOX, DOX@TPE@CLVs **III** or T-DOX@TPE@CLVs **III** for 18 days (mean ± SD, n = 5, P_2* < 0.05). (d) Relative change in bodyweight over time (mean ± SD, n = 5, P_3* < 0.05).

the entire drug-delivery process. Moreover, they were efficacious for tumor therapy *in vitro* and *in vivo*. Tumor growth could be reduced by ~7 times compared with free DOX. Our study provides a novel nano-engineering technology to integrate desired properties (fluorescence, crosslinking, response, and active targeting) in multimodal nanotheranostics.

Conflicts of interest

There are no conflicts of interest to declare.

Acknowledgements

The authors gratefully acknowledge National Natural Science Foundation of China (21975165, 51703145 and 51673130) and China Postdoctoral Science Foundation (2017M620426 and 2019T120844) for financial support. The authors also thank the Center of Testing and Analysis, Sichuan University for TEM measurements.

References

1 K. Kataoka, A. Harada and Y. Nagasaki, *Adv. Drug Delivery Rev.*, 2001, **47**, 113–131.
2 Y. Jiang, D. Cui, Y. Fang, X. Zhen, P. K. Upputuri, M. Pramanik, D. Ding and K. Pu, *Biomaterials*, 2017, **145**, 168–177.
3 H. Chen, W. Zhang, G. Zhu, J. Xie and X. Chen, *Nat. Rev. Mater.*, 2017, **2**, 17024.
4 J. Cao, T. Su, L. Zhang, R. Liu, G. Wang, B. He and Z. Gu, *Int. J. Pharm.*, 2014, **471**, 28–36.
5 C. Li, S. Zhang, J. Pang, Y. Wu and Z. Gu, *Adv. Funct. Mater.*, 2015, **25**, 3764–3774.
6 Y. Matsumura, *Adv. Drug Delivery Rev.*, 2008, **60**, 899–914.
7 M. Talelli, M. Barz, C. J. F. Rijcken, F. Kiessling, W. E. Hennink and T. Lammers, *Nano Today*, 2015, **10**, 93–117.
8 A. Gabizon, R. Catane, B. Uziely, B. Kaufman, T. Safra, R. Cohen, F. Martin, A. Huang and Y. Barenholz, *Cancer Res.*, 1994, **54**, 987–992.
9 K. Cai, X. He, Z. Song, Q. Yin, Y. Zhang, F. M. Uckun, C. Jiang and J. Cheng, *J. Am. Chem. Soc.*, 2015, **137**, 3458–3461.

10 S. Zhang and Y. Zhao, *Bioconjugate Chem.*, 2011, **22**, 523–528.
11 X. Deng, Y. Liang, X. Peng, T. Su, S. Luo, J. Cao, Z. Gu and B. He, *Chem. Commun.*, 2015, **51**, 4271–4274.
12 X. Wang, Y. Yang, Y. Zuo, F. Yang, H. Shen and D. Wu, *Chem. Commun.*, 2016, **52**, 5320–5323.
13 S. Zhang and Y. Zhao, *J. Am. Chem. Soc.*, 2010, **132**, 10642–10644.
14 Y. Chen, J. Huang, S. Zhang and Z. Gu, *Chem. Mater.*, 2017, **29**, 3083–3091.
15 J. Huang, F. Wu, Y. Yu, H. Huang, S. Zhang and J. You, *Org. Biomol. Chem.*, 2017, **15**, 4798–4802.
16 J. Huang, Y. Yu, L. Wang, X. Wang, Z. Gu and S. Zhang, *ACS Appl. Mater. Interfaces*, 2017, **9**, 29030–29037.
17 J. Mei, N. L. C. Leung, R. T. K. Kwok, J. W. Y. Lam and B. Z. Tang, *Chem. Rev.*, 2015, **115**, 11718–11940.
18 X. Xue, Y. Zhao, L. Dai, X. Zhang, X. Hao, C. Zhang, S. Huo, J. Liu, C. Liu, A. Kumar, W.-Q. Chen, G. Zou and X.-J. Liang, *Adv. Mater.*, 2014, **26**, 712–717.
19 C. Li, J. Zhang, S. Zhang and Y. Zhao, *Angew. Chem., Int. Ed.*, 2019, **58**, 1848.
20 C. Liao, Y. Chen, Y. Yao, S. Zhang, Z. Gu and X. Yu, *Chem. Mater.*, 2016, **28**, 7757–7764.
21 J. Zhang, C. Li, C. Liao, P. Zhao, Y. Yu and S. Zhang, *Langmuir*, 2019, **35**, 6676–6682.
22 B. Li, Y. Yu, F. Xiang, S. Zhang and Z. Gu, *ACS Appl. Mater. Interfaces*, 2018, **10**, 16282–16290.
23 Y. Liu, S. Zhu, K. Gu, Z. Guo, X. Huang, M. Wang, H. M. Amin, W. Zhu and P. Shi, *ACS Appl. Mater. Interfaces*, 2017, **9**, 29496–29504.
24 J. Li, R. Cai, N. Kawazoe and G. Chen, *J. Mater. Chem. B*, 2015, **3**, 5806–5814.
25 J. Li, Y. Hu, J. Yang, W. Sun, H. Cai, P. Wei, Y. Sun, G. Zhang, X. Shi and M. Shen, *J. Mater. Chem. B*, 2015, **3**, 5720–5730.
26 N. Li, N. Li, Q. Yi, K. Luo, C. Guo, D. Pan and Z. Gu, *Biomaterials*, 2014, **35**, 9529–9545.